A numerical simulation of a dry-out process for CO_2 sequestration in heterogeneous deep saline aquifers

Jie Ren, College of Civil and Transportation Engineering, Hohai University, Nanjing, China and Lawrence Berkeley National Laboratory, Berkeley, CA, USA

Yuan Wang , College of Civil and Transportation Engineering, Hohai University, Nanjing, China

Yingqi Zhang, Lawrence Berkeley National Laboratory, Berkeley, CA, USA

Abstract

Salt precipitation can be generated near the injection well when dry supercritical CO_2 ($scCO_2$) is injected into deep saline aquifers. Traditional laboratory experiments and numerical simulations focus on the generation of salt precipitation and its impact on core permeability. Recent laboratory experimental studies have shown that the heterogeneity of the core and water content on the surface of the particles plays an important role in the formation of salt precipitation. The goal of this study is to investigate the effects of brine back-flow, heterogeneity, and low water content on salt precipitation. Numerical simulations were performed using core-scale and site-scale models. Simulation results showed the following: 1. Back-flow plays an important role in the salt accumulation near the well – an homogeneous laboratory experiment used with a small core may not provide a full picture of the back-flow phenomenon. 2. The continuous dry-out process reduces the water content near the injection well to zero. As a result, the full range of saturation flow equations should be used to simulate the dry-out process accurately. 3. The heterogeneity of the matrix not only affects the distribution of salt precipitation but also increases the amount of salt precipitation near the well. Homogeneous simulation underestimates the amount of salt precipitation. 4. The reduction in porosity due to salt precipitation could extend the dry-out process in the low permeability zone, further expanding the salt precipitation area.

Keywords: dry-out; back-flow; heterogeneity; low water content; preferential flow; blockage

Introduction

The geological storage of supercritical CO_2 ($scCO_2$) in deep saline aquifers has been proposed to reduce the greenhouse gas effect. Deep saline aquifers are widely distributed in the world and they are considered to have a high storage potential.[1] One of the challenges related to the CO_2 storage in saline aquifers is that, although water is only slightly soluble in a $scCO_2$ flow, a long-time continuous $scCO_2$ injection could cause a considerable loss of liquid water around the injection well.[2] The loss of liquid water will lead to an increase in salt concentration. As a result, salt precipitation will occur when the concentration of brine exceeds the saturation limit.[3] The accumulation of

salt deposits near the injection well could partially block the $scCO_2$ flow path, causing an additional pressure build-up within the injection well.[4]

Many studies on the dry-out problem were carried out based on homogeneous laboratory experiments. Bacci *et al*. used conventional core-flood experiments to study the effect of salt precipitation on absolute permeability (k_a) of the core.[5] They found that the k_a of the core decreased at the end of the experiment after more than 300 pore volumes (PV) of CO_2 were injected into the core. Peysson *et al*. used X-rays to study changes in core permeability caused by salt precipitation and they found that the gas relative permeability (k_{rg}) near the injection part was reduced by 50–70% after sufficient dry gas injection.[6] Typically, the main concern in these projects is the effect of salt precipitation on the $scCO_2$ injectivity (which is characterized by effective permeability k_e, where $k_e = k_a \times k_{rg}$).[7] The core-scale experimental results from Muller *et al*.[8] and Wang *et al*.[9] showed that the salt precipitation causes a significant decrease in the k_e of $scCO_2$, by 60% and 50% in each of the studies, respectively. In contrast, core-scale laboratory experiments carried by Ott *et al*. found that the value of k_a was reduced, while k_e was increased by 20% due to an increase in k_{rg}.[10, 11] The reason provided was that there was no transport mechanism of salt. They believed that salt precipitation was only generated in the part of residual water, maintaining the passage of $scCO_2$-flow.[12] This was similar to the result of Hurter *et al*.[13] According to Hunter *et al*., the local complete evaporation reduced the saturation of residual water to zero under conditions of low salinity, the reduction of liquid phase increases the volume of the $scCO_2$-flow path and thus increased the injectivity of $scCO_2$.

The experiments above were all performed using homogeneous models. In recent years, more and more researchers have started core-scale and pore-scale experiments using heterogeneous models. Ott *et al*. investigated the dry-out problem using heterogeneous rocks.[14] They believed that salt precipitation was not only formed in the residual water but was also forming within the $scCO_2$ flow path due to the capillary-driven transport of brine. To simplify the experimental conditions in heterogeneous cores, Roels *et al*. used two kinds of homogeneous core splices to form one layered heterogeneous core for dry-out experiments. The experimental results showed that the invasion of gas into the low permeability part was rare and the low permeability part contained a large amount of water that stays there because of capillarity. This acted as a water source for the dry-out process in the high permeability part.[7] The capillary pressure gradient moved the water from the low permeability zone to the high permeability zone. Because the low permeability zone serves as a supply of saline water during the dry-out process at the gas-liquid interface, the amount of salt precipitation can increase significantly compared to the homogeneous cores. Similar results were also given in the evaporation experiments.[15] In their experiments, samples were assembled with both coarse and fine particles.[15] Salt precipitation preferentially blocked the surface of the coarse particles, and

the brine water in the fine particles was served as a water source to the evaporation in the coarse particles. Differentiation between evaporation-wicking and drying is important for the generation and accumulation of salt. In the evaporation-wicking situation, in contrast with drying, there is a permanent supply of solution and therefore a steady-state can be reached when the flow rate of liquid sucked into the medium by capillary action exactly balances the evaporation rate.[16] Miri *et al*. conducted pore-scale displacement experiments. They also designed two kinds of pore-system experiments. The experimental results resembled core-scale results.[17] In the homogeneous model, the dry-out will produce only small amounts of salt; in the heterogeneous model, salt precipitation fills the entire gas-flow path.

In site-scale simulations, almost all research on dry-out problems is based on homogeneous systems,[18-23] or considers the saline aquifer as a layered structure, and establishes a simplified heterogeneous system model (inter-layer structural model).[24, 25] Indoor core-scale experiments have revealed the influence of the heterogeneous and the low water content on the salt precipitation formed. Numerical simulations of the salt precipitate phenomenon were performed for homogeneous-system rock formation, and the calculation of salt precipitation mostly adopts the classical capillary pressure equation and the relative permeability equation, which do not take low water content into consideration. These simplifications are reasonable for the qualitative study of the effects of salt precipitation. However, for site-scale simulation, and especially the quantitative evaluation of the effects of the dry-out problem (such as solid saturation and injection well pressure), the accumulation of salt precipitation will be significantly underestimated using traditional equations and an homogeneous system model.[8, 18, 23, 26]

Capillary pressure plays a key role in controlling fluid flow in a multiphase system. In most numerical simulations, static empirical functional relationships are used to calculate capillary pressure and relative permeability.[27-31] However, the experimental studies by Das and Mirzaei have shown that the capillary pressure depends on both water saturation and its time derivative.[32, 33] This is known as the dynamic capillary pressure effect.

In the dynamic capillary pressure model, the time derivative of water saturation is represented by the dynamic coefficient (τ). It quantifies the significance of the dynamic capillary pressure effect. The dynamic coefficient indicates how quickly a two-phase flow system reaches equilibrium. Das *et al*. did a numerical study of the dynamic capillary pressure effect for $scCO_2$-water flow in the porous domain.[34] The results show rising trends for τ as the saturation values reduce. They believed that, for a CO_2-water system, the speed to reach capillary equilibrium (residual water saturation) slows down as the liquid saturation decreases. Goel *et al*. investigated the relationships between the relative permeability curve and the dynamic capillary pressure effects using experimental studies. Their study shows that the relative permeability curve is affected by dynamic effects and provisions must be made in models to include these dynamic

relationships.[35] Simulations had been carried out by Hanspal *et al*. to quantify the effects of temperature (T) on the dynamic capillary pressure and dynamic effects for two-phase flows in porous media.[36] τ was found to be a nonlinear function of water saturation (S_w) and T. A higher temperature led to higher capillary pressure and enhanced residual trapping of CO_2.[37, 38] Their study also concluded that the capillary pressure is affected by various parameters such as time scale, pressure, grain size, and geochemical conditions on the $scCO_2$ injection into deep aquifers.

Most models mentioned above do not include the effects below residual water saturation (S_{lr}) (i.e., $k_{rg} = 1$ in Corey models when $S_w<S_{lr}$).[27] As a result, it becomes increasingly difficult to displace water as the system approaches S_{lr}.[34] However, in reality, a long-time continuous $scCO_2$ injection could cause zero water saturation around the injection well.[2] Webb[39] and Zhang[40] proposed a capillary pressure equation and a relative permeability equation for the corrected full-saturation range (including the fraction of $S_w < S_{lr}$) according to the mobility of the water film. Zhang *et al*. used this full-saturation range capillary pressure equation and relative permeability equation to simulate the salt precipitation in a homogeneous aquifer. The simulation results showed that the solid saturation (S_s) near the well was increased with full-saturation range equations compared to the classical equations.[41] The S_s increased from 0.04 to 0.06 in the Paaratte sand aquifer, from 0.03 to 0.06 in the Berea sand aquifer, and from 0.01 to 0.05 in the Mt Simon sand aquifers. However, the numerical simulation of the heterogeneous aquifer has not been studied using the modified full-saturation range capillary pressure equation and relative permeability equation.

In this paper, we will investigate the accumulation of the salt precipitation using both core-scale and site-scale models. We will focus on the influence of the brine back-flow, low water content, and heterogeneity on the value of S_s, and on how the blockage of pore space due to salt precipitation affects further precipitation. Even though we understand the importance of considering the dynamic effect of the capillary pressure, we use static equations for simplicity as it is not the focus of our study. We currently focus on the effects of capillary pressure at low water saturation ($S_w<S_{lr}$). The influence of dynamic capillary effect on S_s will be considered in future work.

In the discussion below, the core-scale numerical model comes from Roels' experiment.[7] The site-scale model comes from the Sleipner Vest field.[24] There are a total of five models in this article. They are the core-scale short homogeneous model, the core-scale long homogeneous model, the core-scale long layered heterogeneous model, the site-scale homogeneous model, and the site-scale heterogeneous model. Using these models, we examine the effect of the brine back-flow phenomenon on S_s; the effect of low water content on S_s; the effect of heterogeneity on S_s; and the porosity change due to the salt precipitation, which helps to explain how the blockage of pore due to salt precipitation affects further precipitation.

Numerical simulation and results

Model set-up and mesh make

Core-scale models

The prototype of the core-models used in this paper is based on the laboratory experiments by Roels *et al*.[7] The schematic representations of the three core-scale model are shown in Fig. 1. Figures 1a (a short homogeneous model), 1b (a long homogenous model) and the light part of 1c are all Bentheimer sandstone with relatively high permeability. The darker part of Fig. 1c is Berea sandstone, which has a lower permeability than Bentheimer sandstone. The location setup for injection/production wells relative to the surface to the left is the same for all of them. The core-model in Fig. 1c represents a simplified heterogeneous model, made of two homogeneous layers. The core was initially saturated with nearly saturated potassium iodide (KI) solution (58.3 wt%), dry CO_2 injection was initiated with 15 NmL/min under 45°C and 100 bar. An injection of CO_2 would be terminated when there are minor changes in the reduction in pressure for a long period of time (±0.5 bar).[7] Figure 2 shows the distribution of brine saturation (both the presence of brine and solid salt) from CT scan imaging. After the displacement test of three cores, brine saturation in the blue part is close to 0, indicating the onset of the salt precipitation. The figure clearly shows that the solid salt is mainly distributed in the injection well and the outlets.In this study, this physical model is simplified into an X-Y two-dimensional (2-D) numerical model. The grid was generated using the TOUGH2/MESHM module.[42] The size of the model and the location of the well are shown in Fig. 3. All physical boundaries are no-flow boundaries except at the injection well and production well, a constant CO_2 injection rate (Q_{CO2}) (the rate is adjusted from the original rate in the experiment because of the 2-D representation of our model) of 1.7×10^{-5} kg/s is specified, and at the outlets, constant pressure (P) (8 MPa) is specified.

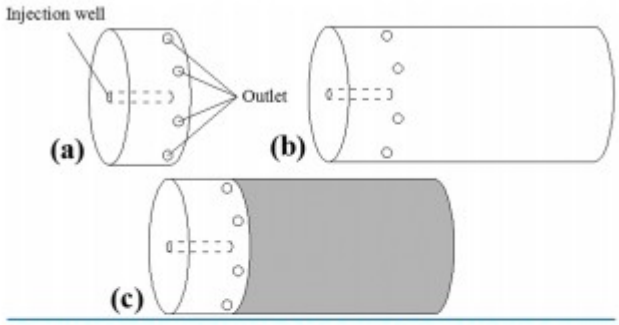

Figure 1. Schematic representation of the core-scale model: (a) short homogeneous core; (b) long homogeneous core; (c) layered heterogeneous core.[7]

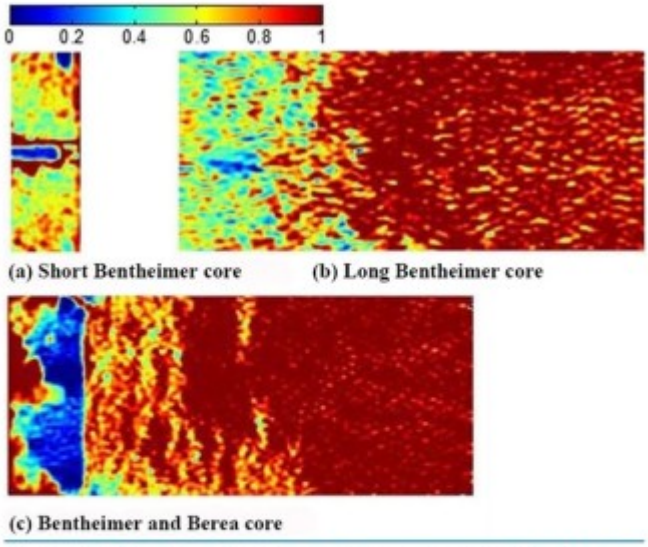

Figure 2. Salt saturation from CT scan imaging: (a) short Bentheimer core; (b) long Bentheimer core; (c) Bentheimer and Berea core.[7]

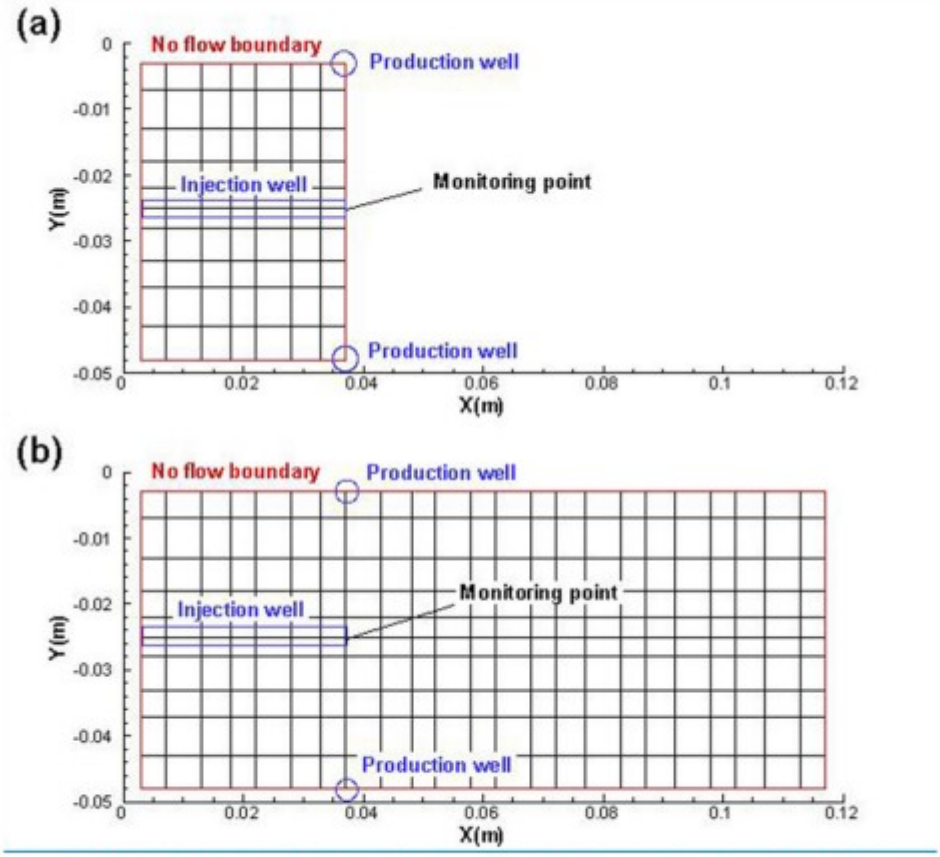

Figure 3. Core-scale simulation model (mesh make and boundary conditions): (a) short core meshing diagram; (b) long core meshing diagram.

Site-scale models

The site-scale conceptual model comes from the first industrial-scale CO_2 disposal project at the Sleipner Vest field. The thickness of the formation at the injection site is 200 m. The injection point is 940 m below the sea floor, and the ocean depth at the site is 80 m. The well is 22 m from the bottom of the aquifer. The model is idealized as a 2-D symmetric domain along Y direction in Fig. 4.[24] The horizontal grid of the model was divided into 58 units. The lengths of the first eight units from the beginning of the injection well were 1, 1, 2, 2, 4, 5, 10 and 15 m respectively, followed by 49 units with the same length of 40 m. The last unit length was 0.001 m (set as a constant pressure boundary). The vertical grid of the model was divided into 50 units. The heights of the well and the upper unit of the well were both 2 m; the other 48 units were all 4 m in height. The distance between the injection well and the lower boundary was 22 m (as seen in Fig. 4). The geological data came from the Geostatistical Software Library and UserSoftomje (GSLIB).[43] The data were divided into four groups according to the size of the permeability value. The top 30% of the size of the permeability values were grouped together and called sand 2, the second

largest 40% of the permeability values in the were grouped together and called sand 1, the smallest 10% of the permeability values were grouped together and called sand 4, and the remaining 20% of the data were grouped together and called sand 3. The facies distribution of the model is given in Fig. 5. On the other hand, the homogeneous model was established to compare with the heterogeneous model, the rock type in the homogeneous model was set as sand 2 (which have biggest permeability value group in GSLIB's data).

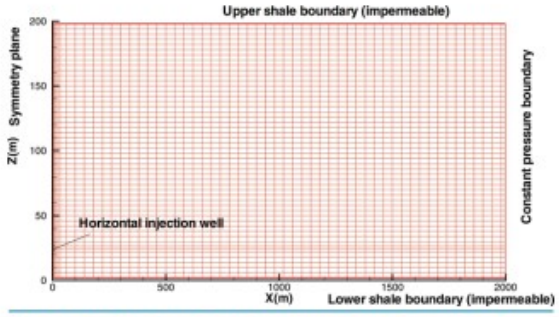

Figure 4. Site-scale simulation model (mesh make and boundary conditions), a 1 m thick section perpendicular to the horizontal well is considered.

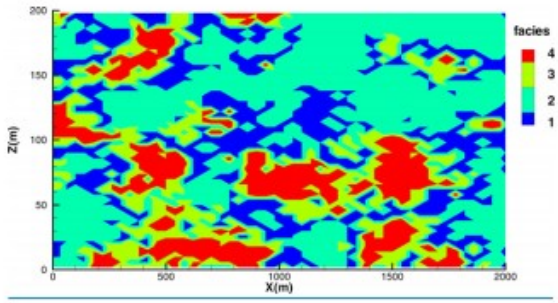

Figure 5. Heterogeneous facies distribution according to the permeability value.

Model parameter settings

The static capillary pressure function used the van Genuchten model:[31]

$$P_c = -P_0\left(\left[S^*\right]^{-1/\lambda} - 1\right)^{1-\lambda} \qquad (1)$$

where, P_c[Pa] is the capillary pressure, P_0[Pa] is the air-entry pressure, S^*[-] is the effective saturation, $-\square max \leq \square c \leq 0 - Pmax \leq Pc \leq 0$, P_{max}[Pa] is the maximum capillary pressure, $\square * = (\square l - \square lr)/(\square ls - \square lr) S* = (Sl - Slr)/(Sls - Slr)$, S_l[-] = S_w[-] in this study, S_{ls}[-] is the liquid saturation in saturated state, $\square = \square = 1 - 1/\square \lambda = m = 1 - 1/n$, λ[-], m[-], and n[-] are parameters related to pore-size distribution.

The relative permeability function used the Van Genuchten-Mualem model:[31, 44]

$$k_{rl} = \begin{cases} \sqrt{S^*}\left\{1 - \left(1 - [S^*]^{1/\lambda}\right)^{\lambda}\right\}^2 & \text{if } S_l < S_{ls} \\ 1 & \text{if } S_l < S_{ls} \end{cases} \qquad (2)$$

Gas relative permeability used the Corey function:[27]

$$k_{rg} = \left(1 - \hat{S}\right)^2 \left(1 - \hat{S}^2\right) \text{ if } S_{gr} > 0 \qquad (3)$$

where, k_{rl}[-] is the liquid relative permeability, $0 \leq k_{rl}, k_{rg} \leq 1$, $\widehat{S}$ [-] is the effective saturation in the relative permeability

functions, $\widehat{S} = (S_l - S_{lr}) / (1 - S_{lr} - S_{gr})$, S_{gr}[-] is the residual gas saturation. Plots of the capillary pressure equation and the relative permeability equation are given in Fig. 6 and Fig. 7, respectively. The parameters in the numerical simulation are presented in Table 1. In this article we do not consider the temperature change and keep the system as an isothermal condition.

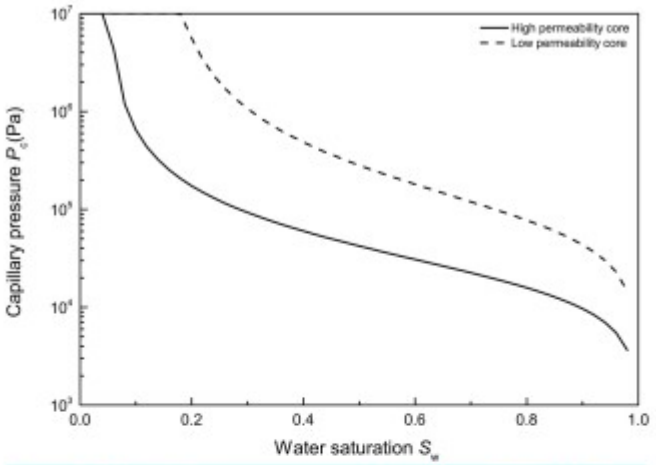

Figure 6. Capillary pressure curve for different part of the core.

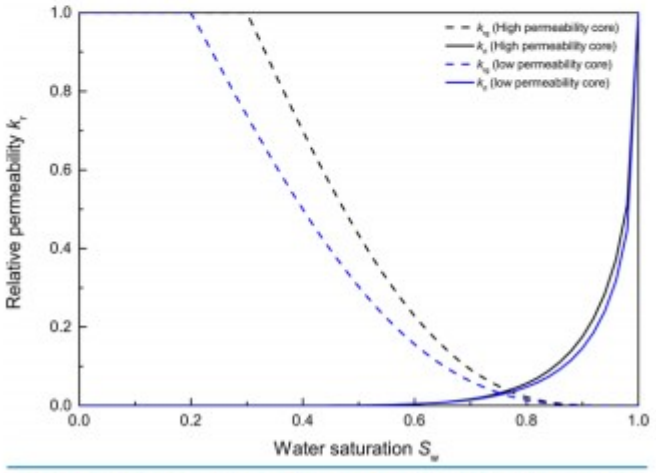

Figure 7. Relative permeability curve for different part of the core.

Table 1. The parameters of the model.

Parameter type		Parameter values
High permeability core	permeability	$k_x = 100$ mD, $k_y = 100$ mD, $k_z = 100$ mD
	porosity	$\phi = 12\%$
	Parameters in the relative permeability function	$m = 0.457$, $S_{lr} = 0.30$, $S_{ls} = 1.0$, $S_{gr} = 0.05$
	Parameters in the capillary function	$m = 0.457$, $S_{lr} = 0.05$, $1/P_0 = 5.1 \times 10^{-5}$, $P_{max} = 10$ MPa, $S_{ls} = 0.999$
Low permeability core	permeability	$k_x = 0.1$ mD, $k_y = 0.1$ mD, $k_z = 0.1$ mD
	porosity	$\phi = 6\%$
	Parameters in the relative permeability function	$m = 0.40$, $S_{lr} = 0.20$, $S_{ls} = 1.0$, $S_{gr} = 0.05$
	Parameters in the capillary function	$m = 0.40$, $S_{lr} = 0.05$, $1/P_0 = 1.25 \times 10^{-5}$, $P_{max} = 10$ MPa, $S_{ls} = 0.999$
Initial conditions		$P = 8$ MPa, $X_{NaCl} = 0.15$, $S_g = 0.0$, $T = 60$°C
Neumann boundary condition		$Q_{CO2} = 1.7 \times 10^{-5}$ kg/s
Injection time		24 h

The effect of brine back-flow on S_s

The back-flow phenomenon plays an extremely important role in the formation of salt precipitation.[18] In the process of continuously displacing saline water with $scCO_2$, the CO_2 saturation of the rock formation gradually increases and the liquid saturation gradually decreases. The capillary pressure at the wall of the injection well causes saline water to flow back to the injection well when the capillary pressure exceeds the displacement pressure.

Short homogeneous core model

The short core model in Figure 3a is used for simulation in this section. We used the TOUGH2/ECO2N module to simulate experiments that injected CO_2 into a short homogeneous core.[24] The EOS module considers three phases: a liquid phase, a CO_2-rich gas phase, and solid salt. The observed variables include gas saturation (S_g), solid saturation (S_s), and pressure (P). The simulation time was 24 hours (continuous CO_2 injection for 24 hours at a constant rate 1.7×10^{-5} kg/s). To understand how back-flow affects salt precipitation, we performed two numerical simulations. We ignored capillary pressure (and ignored the back-flow phenomenon) at first, and then added the capillary pressure function into the simulation (Eqn 1). The parameters used in this section are given in Table 1 (the part of high permeability core).

The contour map of S_s after 24 h (1 day) simulation is shown in Fig. 8. We chose the end of the horizontal injection well as the monitoring point. Figure 9 shows the time evolution of the S_s.

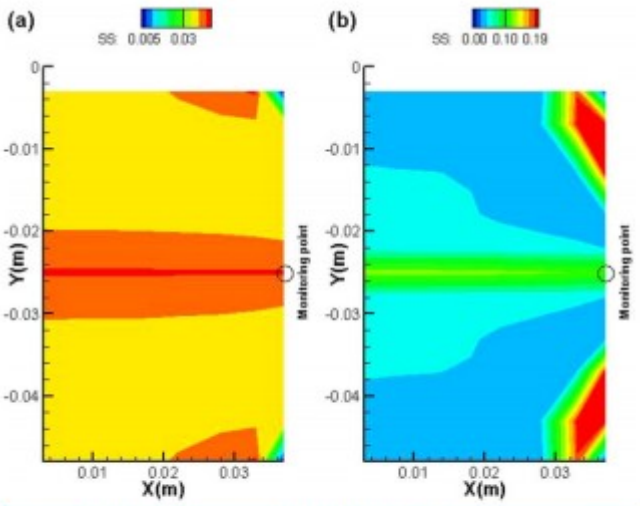

Figure 8. Simulation results of the short homogeneous core (black circle in the figure is the monitoring point): (a) no capillary pressure; (b) with capillary pressure.

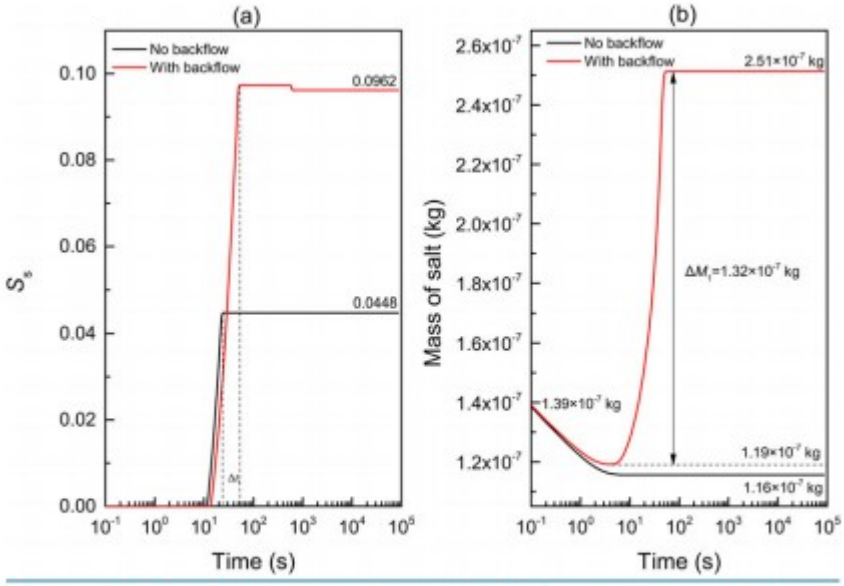

Figure 9. Time evolution of S_s and mass of salt at the monitoring point in same short homogeneous model: (a) time evolution of S_s at the monitoring point; (b) time evolution of mass of salt at the monitoring point.

After the core reaches the residual liquid saturation, the dry $scCO_2$ injection into the core will dissolve the water from the residual brine out of the core, causing an increase in the mass fraction of salt in the liquid phrase, eventually leading salt to precipitate when it reaches the saturation limit. In this article, the salt precipitation is observed in terms of S_s. Figure 8 shows simulation results of S_s at the end of the simulation. In the simulation, the solid phase already starts to appear in the injection well because the TOUGH2 model uses an equilibrium assumption (although in the real

experiment it takes some time for salt to precipitate). The S_s is abnormally large at the outlet in Fig. 8; this may be due to the capillary end effect during the flooding experiment (Due to capillary forces, the saturation of the wetting phase (water) is abnormally high at the core outlet, compared to the normal saturation at the core.)[45]

The values of the S_s near the well are in the range of 0.005 to 0.045 (Fig. 8a), much lower than 0.02 to 0.18 in Fig. 8b. That is because there is no-counter flow of liquid due to capillary pressure. The salt precipitation resulting from the dry-out effect is from the *in situ* brine near the well, and there is no additional brine supply from the adjacent region. In Fig. 9a, the S_s value in the monitoring point (black circle in Fig. 8) with the capillary-derived back-flow (0.0962) is almost twice the value of simulation that ignore the back flow (0.0448). The back-flow phenomenon makes the dry-out process at the monitoring point extend Δt_1 times and significantly increased the amount of precipitation. The salt mass in the element of monitoring point as a function of time is shown in Fig. 9b. In Fig. 9b, salt mass is reducing during the initial time of CO_2, indicates the viscous drainage process. The mass of salt at the monitoring point is 1.39×10^{-7} kg under the initial conditions. The salt mass will decrease to 1.16×10^{-7} kg when there is no brine backflow to the monitoring point, and there is no increasing trend of salt. However, the salt mass will increase from 1.19×10^{-7} kg to the stable maximum value (2.51×10^{-7} kg) when the capillary pressure is considered in the simulation, this additional salt increase at the monitoring point is due to the back-flow phenomenon. The back-flow mass of salt (ΔM_1) in the monitoring point is about 1.32×10^{-7} kg.

Long homogeneous core model

We return to the situation with the capillary pressure. The size of the laboratory core is small and the amount of saline water contained in the pores is relatively small because of the restriction of the core-scale experimental condition. The long homogeneous core simulation is carried out to understand how the S_s changes with the core size (the amount of the total water content). The long core model in Fig. 3b is used for simulation in this section. Simulation parameters of the long homogeneous core were consistent with that of the short homogeneous core. The monitoring point in the two models is shown in Fig. 3. The time evolution of S_s and mass of salt in the monitoring point is shown in Fig. 10.

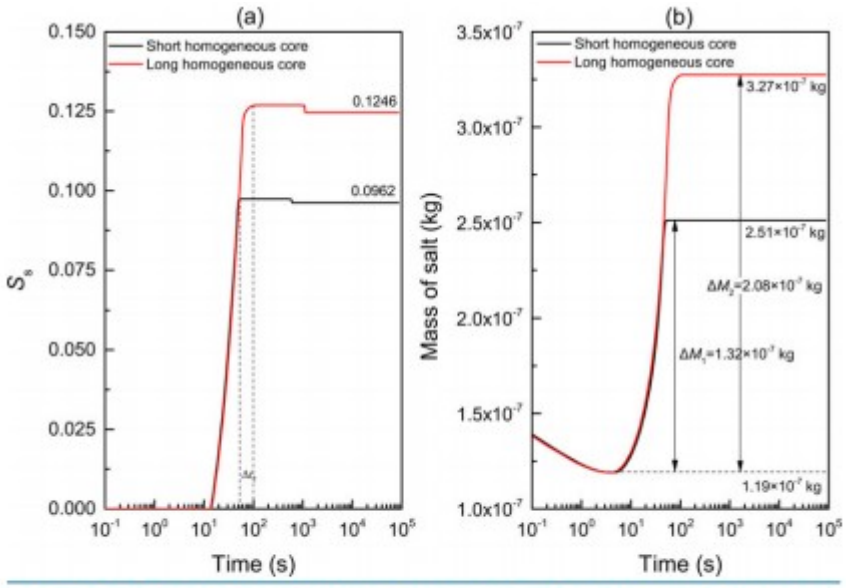

Figure 10. Time evolution of S_s and mass of salt at the monitoring point in different homogeneous model: (a) time evolution of S_s at the monitoring point; (b) time evolution of mass of salt at the monitoring point.

In Fig. 10a, the value of the S_s in the long homogeneous core at the monitoring point is nearly 0.1246. The increase is significant compared with the value in the short homogeneous core (0.0962). On the other hand, the core-size extension increased the time length (Δt_2) of the dry-out process at the monitoring point. In Fig. 10b, the back-flow mass of salt (ΔM_2) in the monitoring point is about 2.08×10^{-7} kg in the long homogeneous core, larger than that in short homogeneous core ($\Delta M_1 = 1.32 \times 10^{-7}$ kg). As Fig. 3a shows, the back-flow of brine in the monitoring point is mainly from upper and lower parts of the core. In Fig. 3b, in addition to the upper and lower parts of the core, the right side of the core also provides back-flow water to the monitoring point. The results show that increasing the size of the core makes the precipitation of salt increase noticeably. The core-scale experiment is limited by the size of the core holder, so the amount of brine available for capillary back-flow is limited.

Table 2 shows the results of salt precipitation on core-scale homogeneous laboratory experiments in recent years. The results obtained by different scholars are different for the effects of salt precipitation.
Ott *et al*.[10] concluded that the rise of k_e is contrary to the conclusions of other scholars.[5, 6, 8, 9] Considering $k_e = k_a \times k_r$, a decrease of k_a and k_r should result in a decrease in k_e. In the results of Ott *et al*., the decreases in k_a and the increase in k_e are attributed to an increase in k_{rg}.[10] Salinity (X_{NaCl}) is the most critical parameter in the parameter sensitivity analysis that affects the value of solid saturation.[23] For different cores, the time of injection and the size of the core also make the amount of salt precipitation different, mainly due to the influence of the dry-out time and relative amount between water and salt. Comparing these researchers' experimental conditions, it is found that

the core size is too small (two orders of magnitude) and the displacement time is shorter (8.5 h) in the experiments of Ott *et al*. (although the X_{NaCl} = 20% is sufficiently high in the experiment).[10] This small size of the core results in the small amount of saline water available for back-flow. The saline water in the core may not reach the completely dried-out state in a short time. Uncertain results about the influence of salt precipitation may be found when examining the homogeneous core-scale laboratory experiments.

Table 2. Permeability change in core-scale laboratory experiments and parameter conditions.

Publication	Permeability change	Salinity (X_{NaCl}) (%)	Injection time (h)	Core size (m^3)
Muller *et al.*[8]	k_e reduced by 60%	25	32	1.37×10^{-4}
Bacci *et al.*[5]	k_a reduced by 30–86%	13	16	5.52×10^{-4}
Peysson *et al.*[6]	k_r reduced by 50–70%	3, 13, 14	800	1.13×10^{-4}
Wang *et al.*[9]	k_e reduced by 50%	25	19	3.30×10^{-4}
Ott *et al.*[10]	k_e increased by 5 times	20	8.5	3.93×10^{-6}

In the short homogeneous model simulation, brine is brought back due to capillary pressure as the supply of salt for the continuous dry-out process near the well. But this does not reach the limit of capillary back-flow at the monitoring point. In the long homogeneous model simulation, more brine water is brought back to the same location. The results of the long homogeneous model simulation indicate that the small size of the homogeneous core underestimates the amount of salt precipitation, which may be the reason why the laboratory experiments in the core scale have different results about salt precipitation.

The effect of low water content on S_s

The brine formation facilitates a two-phase flow system in which mobile water is replaced by the injected dry $scCO_2$. Eventually, the immobile residual water is trapped in pores or on the grain surface as a thin film.[46] The contribution of the film to the total displacement process is generally very small and negligible under saturated conditions. However, when the soil is very dry and the flow becomes very small, the film can be significant or even dominant.[47] We divide the capillary pressure curve into two parts: part 1 for $S_w \geq S_{lr}$, and part 2 for $S_w < S_{lr}$. The models that consider dynamic capillary effect do not include part 2 because the capillary equilibrium state is reached when $S_w < S_{lr}$.[34] However, the time it takes for the system to reach the equilibrium state in part 1 is affected by dynamic capillary effects. As a result, even the evaporation process of the residual brine mainly occurs in part 1; the dynamic capillary effect may still have an influence on salt accumulation, and therefore the amount of back-flow brine when $S_w < S_{lr}$. This effect will be considered in future work.

The van Genuchten (vG) model is commonly used in the numerical simulation of $scCO_2$ sequestration.[31] In the vG model, the liquid relative permeability approaches zero and the capillary pressure goes to infinity when the liquid saturation approaches the residual water saturation. The

calculation is usually given a cut-off value on the capillary pressure curve, called the maximum capillary pressure value (P_{max}). As shown in Fig. 6, the P_{max} value is 10^7 Pa in our simulation. However, a long injection of dry $scCO_2$ can reduce the water saturation below its residual value, at which point the contribution from the film flow can become significant or even dominant.

The pore system can reach a fully dry condition. Consider the capillary pressure and relative permeability equations with full-range water content, in which the residual water saturation can be lowered to 0. Using the full-range saturation capillary pressure and relative permeability equations helps obtain an accurate solid saturation value, especially for the dry-out zone near the injection well. The capillary pressure equation is based on the classical capillary pressure equation and log-linear extension to the full range of saturation:[48, 49]

$$P_c = \begin{cases} -\frac{1}{\alpha}\left[(S_{ec})^{(\gamma-1)/m} - 1\right]^{1/n}, \\ \qquad S_l \geq (S_{lr} + \varepsilon) \\ -\frac{1}{\alpha}\left[S_{ec^*}^{(\gamma-1)/m} - 1\right]^{1/n} - \beta\,(S_l - S_{lr} - \varepsilon), \\ \qquad S_l < (S_{lr} + \varepsilon) \end{cases} \quad (4)$$

where, α[-] is the parameter related to P_0, and γ[-] is the parameter of the active fracture model.[48] $S_{ec} = (S_l - S_{lr})/(1 - S_{lr})$, S_{ec}[-] is the effective saturation of classical function part in this function. $S_{ec^*} = \varepsilon/(1 - S_{lr})$, S_{ec^*} is the effective saturation of the extension function part in this capillary pressure function, and ε[-] is the difference between residual water saturation in the classical capillary pressure function and the extension point in this capillary pressure function (Fig. 11). β[-] is the expansion factor, $\beta = -\log_{10}(e) \cdot \left(\frac{1-m}{m} \cdot \frac{\gamma-1}{\varepsilon} \cdot \frac{1}{S_{ec^*}^{(1-\gamma)/m} - 1}\right)$. The full range of saturation relative permeability equations is as follows:[49]

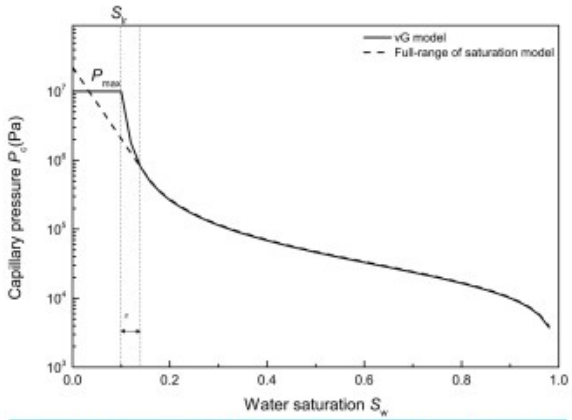

Figure 11. Comparison between the classical and modified full-range of saturation capillary equation.

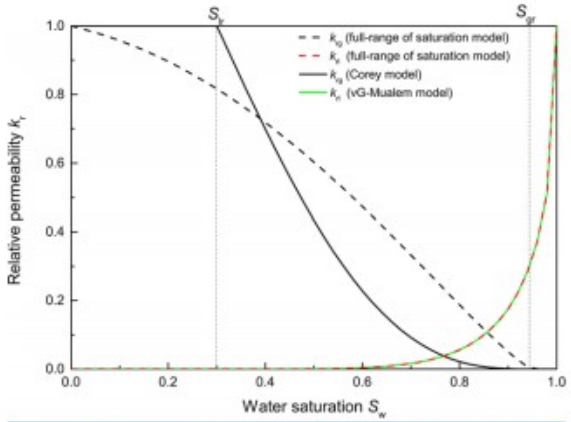

Figure 12. Comparison between the classical and modified full-range of saturation relative permeability equation.

The short homogeneous system core in Fig. 3a is used to investigate how full-range, full-liquid formulation affects simulation results. The simulation results are compared with the results from Eqns 1, 2, and 3. The parameter settings are consistent with the previous simulation in the section on the short homogeneous core model above. The parameters of the full range of the saturation capillary equation and relative permeability equation are given in Table 3 (high permeability part), and the simulation results are given in Fig. 13.

Table 3. The parameters of the full range of saturation capillary equation and relative permeability equation.

Rock type	Parameter type	Parameter values
High permeability core	Parameters in the relative permeability function	$S_{lr} = 0.3$, $S_{gr} = 0.05$
	Parameters in the capillary function	$n = 1.84$, $1/\alpha = 20000$ Pa, $\varepsilon = -0.03$
Low permeability core	Parameters in the relative permeability function	$S_{lr} = 0.2$, $S_{gr} = 0.05$
	Parameters in the capillary function	$n = 1.67$, $1/\alpha = 80000$ Pa, $\varepsilon = -0.05$

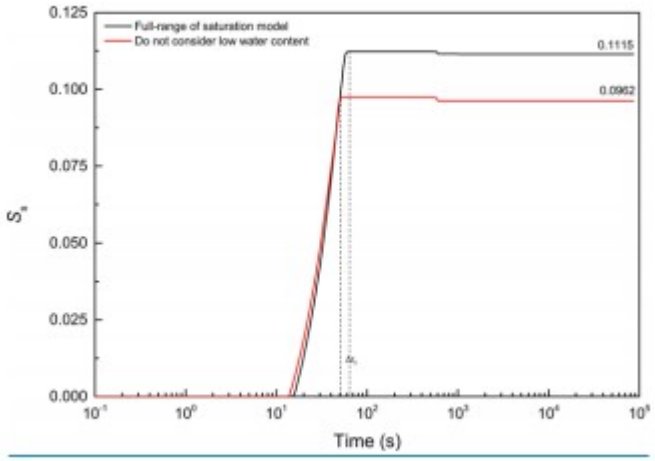

Figure 13. Time evolution of S_s in two cases.

In Fig. 13, salt precipitation at the monitoring point is significantly increased by using the modified full range of saturation equations. The S_s value keeps at 0.1115 by using modified equations, and 0.0962 by using unmodified equations. Simulation of the dry-out process continues more time (Δt_3) by using modified equations than by using unmodified equations. This added time mainly comes from the evaporation of the low water content.

As seen in Fig. 12, k_{rg} becomes 1 and k_{rl} becomes negligible when $S_w < S_{lr}$ in the Corey model. During a short period of time (e.g., minutes to days for many laboratory experiments), some small k_{rl} values may not matter much in terms of generating meaningful volumes of aqueous flow. However, over a long period, the cumulative effects of these same small values may not be negligible.[41] In this study, the cumulative effect of k_{rl} makes the S_s increase 0.0153 at the monitoring point for a 1-year simulation (Fig. 13).

These simulation results show that low water content in the dry-out process should not be ignored during the numerical simulation, especially for the longtime injection process simulation. The full range of capillary function and permeability function should be chosen when it comes to dry-out problem simulations near the well, because this area would become a completely dry condition. An equation that does not consider low water content would underestimate the amount of salt precipitation.

The effect of heterogeneity on S_s

Core-scale heterogeneous simulation

In a laboratory experiment, we set the temperature, flow rate, and pressure conditions similar to the site in order to bring the experimental conditions close to the actual situation at the site. In the actual field, the rock is surrounded by other water-bearing rocks, these water-bearing rocks can serve as the brine source when brine water flow back to the evaporation area. Due to the size of the experimental apparatus, such brine sources are usually neglected. Many scholars have studied the migration characteristics of $scCO_2$ after $scCO_2$ injection into the saline aquifers. They believe that the preferential flow of $scCO_2$ is the most important migration characteristic.[50, 51] In general, $scCO_2$ will preferentially migrate into high-permeability rock during the displacement process, and only a small amount of $scCO_2$ will flow into the low-permeability rock. Lower permeability rock can serve as the brine source for high permeability rock.

The long core model in Fig. 3b is used for simulation in this section. The parameters in the numerical simulation are presented in Table 1, but parameters in relative function and capillary function are given in Table 3 (low water content is considered). Figure 14 shows the contour map of S_g in the long homogeneous core simulation. Figure 15 shows the contour map of S_g in the long heterogeneous core simulation. Contour maps of S_g are selected in three simulation times to express gas move trends. Figure 16 shows the contour map of S_s after 24 hours simulation in the

homogeneous and heterogeneous model. We chose the whole left part of the model as the monitoring part. The time evolution of the total mass of salt in the left part of the model is shown in Fig. 17.

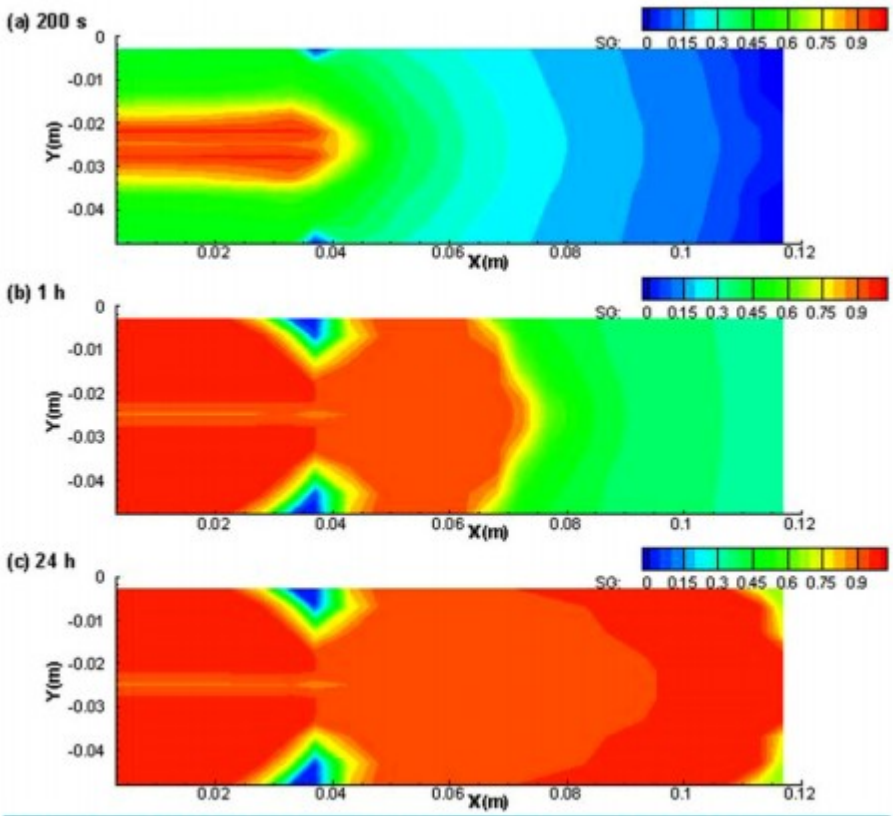

Figure 14. Contour map of S_g in the long homogeneous core simulation: (a) 200-second simulation; (b) 1-hour simulation; (c) 24-hour simulation.

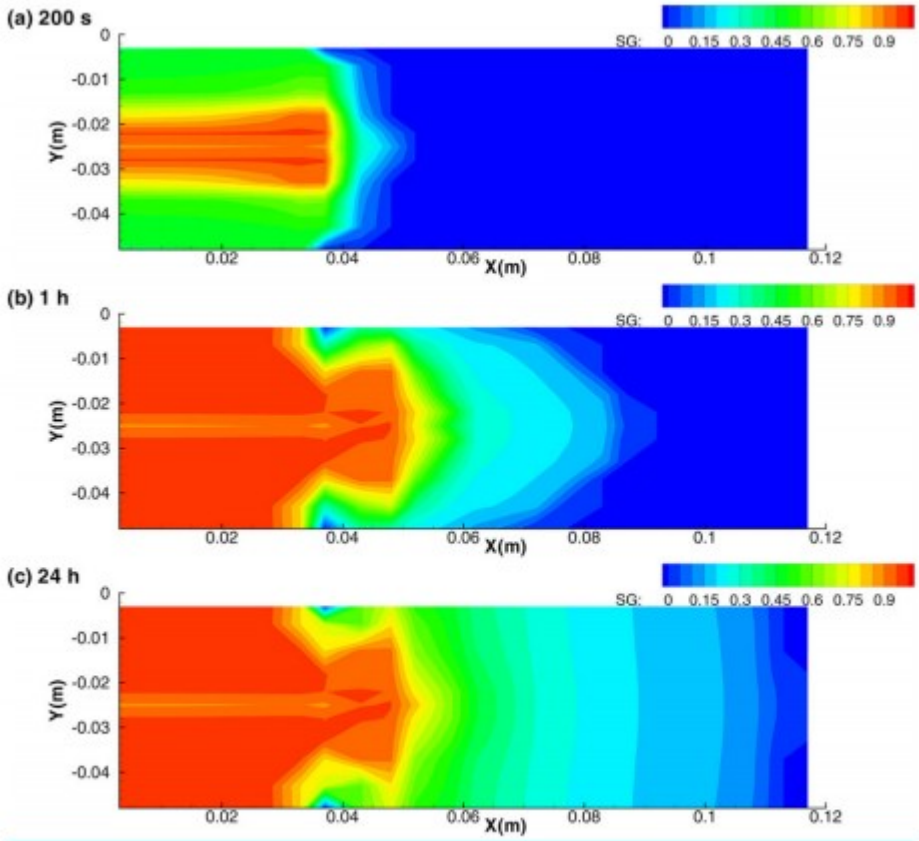

Figure 15. Contour map of S_g in the long heterogeneous core simulation: (a) 200-second simulation; (b) 1-hour simulation; (c) 24-hour simulation.

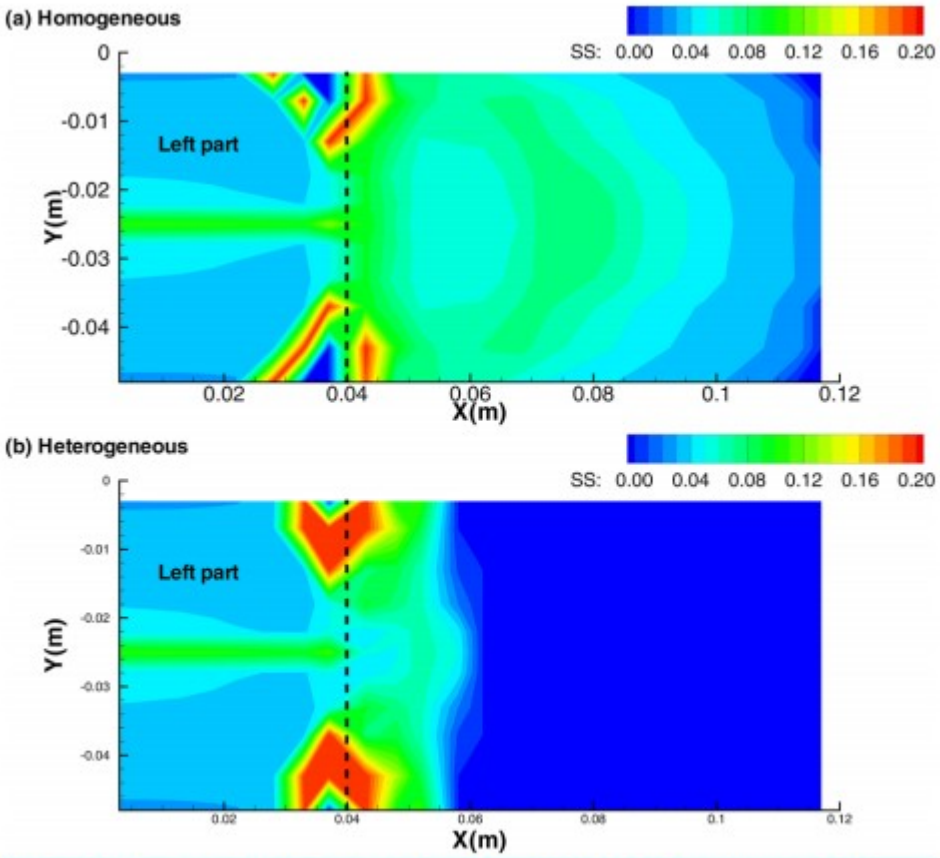

Figure 16. Contour map of S_s after 24 hours' simulation in the homogeneous and heterogeneous model, respectively: (a) homogeneous model; (b) heterogeneous model.

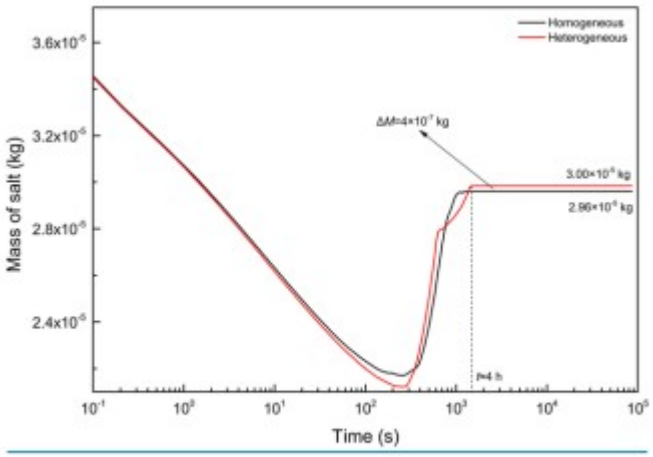

Figure 17. Time evolution of total mass of salt in the left part of the model

In Fig. 14, the gas phase gradually fills the entire core from the injection well to the end of the core. However, in the layered heterogeneous core, the gas phase invades the left larger permeability part first, keeping the low

permeability party as the brine source (low gas saturation) (Fig. 15a). After the gas fills the high permeability part, it gradually invades the low permeability part (Fig. 15b and Fig. 15c). The layered heterogeneous structure provides a preferential flow passage to the gas phase. Figure 16a and Fig. 16b are the contour map of S_s at the end of the experiment of the homogeneous core and layered heterogeneous core, respectively. In Fig. 16a, the solid almost occupies the entire model. In Fig. 16b, salt precipitation accumulates mainly at the interface of the two rocks and the left part of the model (the high permeability zone), which corresponds to the gas flow path. In the layered heterogeneous core, the left part of the core is completely dry, and the majority of the right part of the core still remains fully saturated with liquid. The high solid saturation (S_s = 0.18~0.20) area in Fig. 16b is larger than that in Fig. 16a, which reveals the influence of heterogeneity.

The evolution of the total mass of salt over time at the monitoring part in both models is given in Fig. 17. After 4 hours' simulation, there is not much change in the mass of salt in the left part, which indicates that the left part of two models has been dried out completely. There is an additional mass of salt gathering ($\Delta M = 4 \times 10^{-7}$ kg) in the left part of the heterogeneous model comparing to the homogeneous model. This increase is mainly due to heterogeneity; the low permeability zone provides additional water and salt for the dry-out process in the left part.

The numerical results are similar to the CT scan results from laboratory experiments by Roels *et al*. (Fig. 2).[7] The blue part characterizes the distribution of salt precipitates, and the salt deposits accumulate at the rock interface of the two rocks (Fig. 2c). The low permeability Berea sandstone provides salt water for the dry-out process of the Bentheimer sandstone as reservoir brine. This resulted in the accumulation of salt precipitation near the injection well in the heterogeneous system core (Fig. 2c) more than in the homogeneous system core (Fig. 2b).

The accumulation of salt precipitation in the presence of a brine reservoir has been verified by many scholars in laboratory experiments. Most of the heterogeneous systems are fracture-matrix systems in laboratory experiments, except those of Roels *et al*.,[7] who included a core-scale laboratory experiment[52] and a pore-scale laboratory experiment.[17] Setting the heterogeneous system as a fracture-matrix system simplifies the experimental process. The rapid flow of gas in the fracture helps to form the preferential flow and brine source rapidly. This accelerates the evaporation process and increases the amount of brine reservoir. However, the fluid flow in the fracture may have been a non-Darcy process. Using the fracture-matrix system may not be accurate compared to the heterogeneous system.

The heterogeneity of the matrix not only affects the distribution of salt precipitation but also the amount of salt precipitation. Results from the core-scale heterogeneous model simulation show that the heterogeneity of the

core can cause the preferential flow of water and CO_2 during the dry-out process. The extra brine in low permeability regions could serve as a brine source to supply the brine for the dry-out process near the well. This leads to an increase in the amount of precipitation in the preferential flow region.

Site-scale heterogeneous simulation

Under real site conditions, the deep saline aquifer is strongly heterogeneous because of the discontinuity of the rock deposition process. Carle proposed a geological modeling method based on facies classification in 1999.[53] Different facies had different levels of porosity and permeability. The dry-out process in the heterogeneous core can be considered as the evaporation process under the brine reservoir consideration. In the numerical simulation of the dry-out near the injection well, results from the heterogeneous model are more realistic than those from homogeneous models. In this section, we discuss some site-scale simulation results from a heterogeneous model based on multi-facies theory, considering the back-flow and the full range of water content. The specific process is as follows.

The injection rate of $scCO_2$ (Q_{CO2}) was set at 0.25 kg/s (2600 Mt/year) in the numerical simulation, and the injection duration was 1 year. The other parameters were the same as the numerical simulation parameters in the ECO2N sample (rtp7).[24] The result of the numerical simulation is shown in Fig. 18, Fig. 19, and Fig. 20.

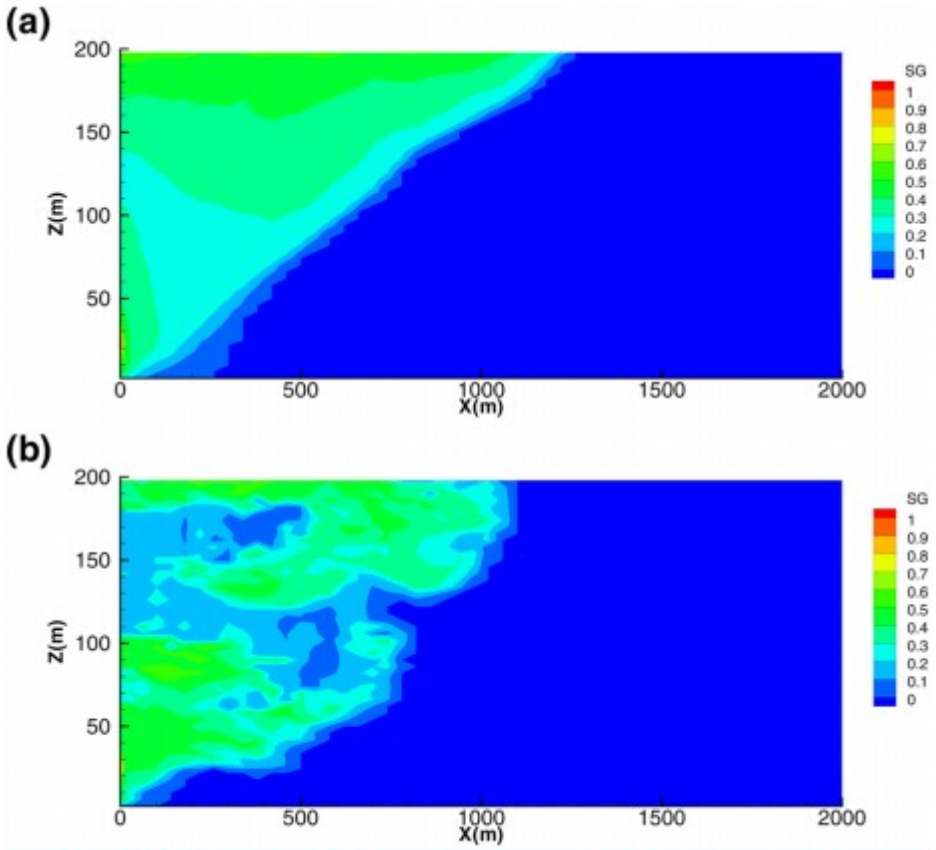

Figure 18. Contour maps of S_g, (a) homogeneous model; (b) heterogeneous model.

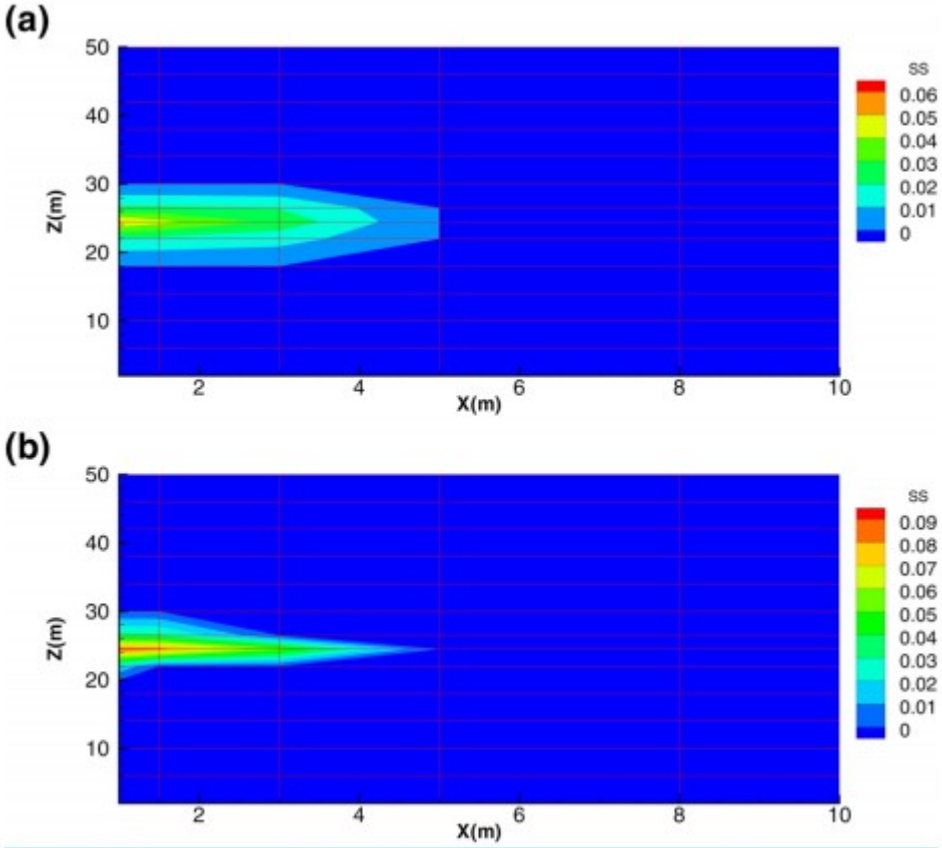

Figure 19. Contour maps of S_s near the well: (a) homogeneous model; (b) heterogeneous model.

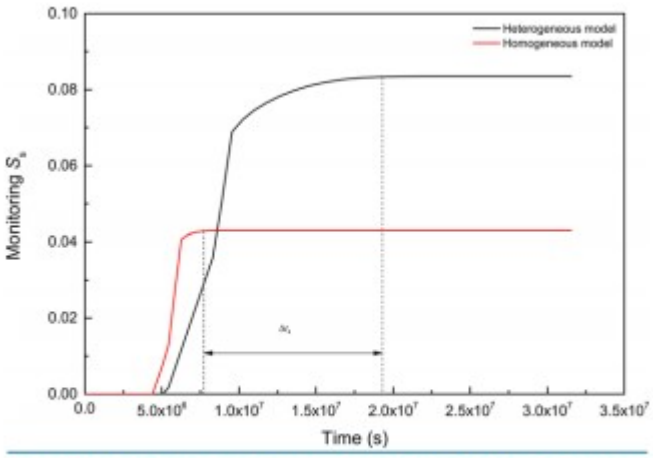

Figure 20. Comparison of S_s of the injection well between homogeneous and heterogeneous models.

Figure 18 is the contour map of S_g in two different models after the end of the injection process. In Fig. 18a, the distribution of $scCO_2$ is mainly affected by the buoyancy in the homogeneous model simulation. The $scCO_2$ migrates upward to gather at the upper boundary, forming the shape of the funnel. In

Fig. 18b, in addition to the shape of the funnel, there are several low S_g zones in the contour map of gas distribution due to the capillary barrier. These low S_g zones indicate the brine source and are surrounded by the high S_g zone. Mainly because of the $scCO_2$, these low S_g zones prefer to pass the high permeability zone to form a preferential flow phenomenon. This migration process causes the gas to enclose the saline water partially and form a partial seal of the water. Figure 19 is the contour map of S_s near the injection well in two different models after the end of the injection process. The shape of the S_s contour map of the homogeneous model is more or less symmetrical up and down, however, the shape of the S_s contour map of the heterogeneous model is obviously asymmetric. In a homogeneous model, the range of high S_s zone is 0 to 1.5 m with a value of 0.06; in a heterogeneous model, the range of high S_s zone is 0 to 2 m with a value of 0.085. The previous section revealed that water in the low permeability zone acts as a brine source for the dry-out process, which makes an additional dry-out process near the injection well.

Figure 20 shows the relationship between S_s and injection time at the injection well in two different models. In Fig. 20, a value of S_s simulated by the heterogeneous model is twice as much as that simulated by homogeneous model, the amount of salt precipitation has a significant increase due to the movement of the brine water in the heterogeneous system. The dry-out process in the heterogeneous model has a longer duration (Δt_4) than that in the homogeneous model, which is due to the brine source formed by the preferential flow in the heterogeneous model.

The parameter related to pore size distribution (m) is often used to characterize the heterogeneity of rock in the classical homogeneous model. Some researchers changed the value of m to do the sensitivity analysis about the dry-out problem. However, they used the homogeneous model to do the sensitivity analysis; they believed that heterogeneities do not appear to play a major role in the amount of salt precipitation and the solid distribution.[23, 46] But we think that this numerical simulation underestimates the amount of solid precipitation near the injection well. The heterogeneous model simulation should be used to predict the effect of solid precipitation in a site-scale numerical simulation. A heterogeneous model is a more realistic representation of the effects of salt precipitation in the field-scale simulation. Correct simulations of the distribution of gas phase and solid phase, as well as the maximum solid saturation value near the injection well, are important for understanding well injectivity.

How salt precipitation induced porosity change affects further precipitation

In previous simulations, we only considered the change in S_s and mass of salt in the model; we did not consider the porosity or permeability changes due to the salt precipitation. TOUGH2/ECO2N provides some options for accommodating the permeability change due to precipitation.[24] We used the tubes-in-series model to do a site-scale simulation.[54] The contour map of S_s is

shown in Fig. 21. The injection well is the observation point, and pressure as a function of time in two different cases is shown in Fig. 22.

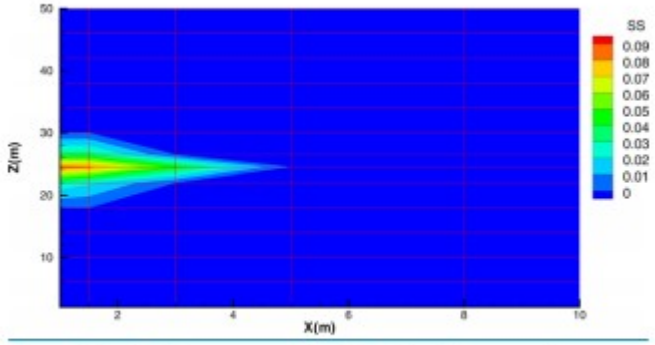

Figure 21. Contour map of S_s. Consider the porosity or permeability change due to the salt precipitation.

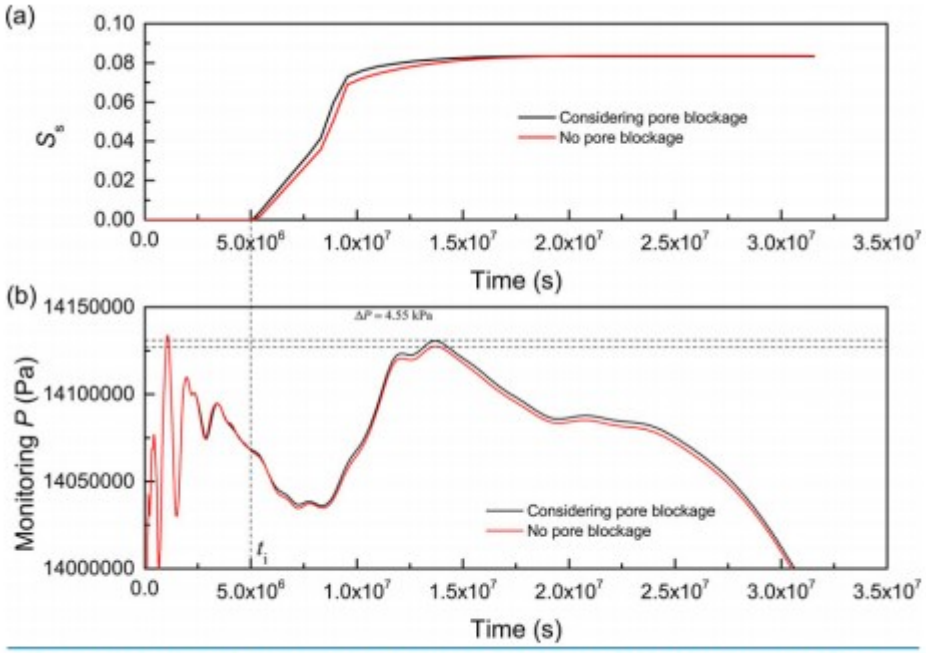

Figure 22. Time evolution of P and S_s at the injection well: (a) time evolution of S_s; (b) time evolution of pressure.

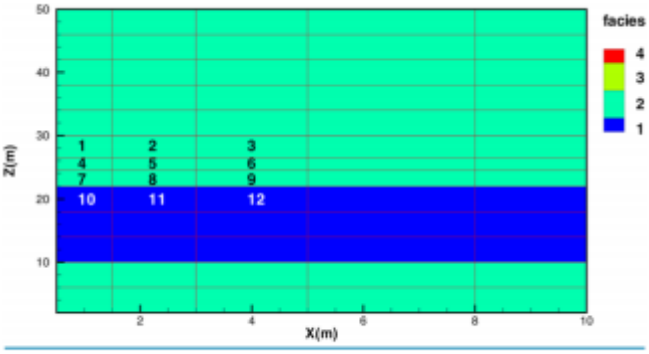

Figure 23. Facies distribution near the injection well.

Figure 21 is the contour map of S_s by considering the porosity or permeability changes due to the salt precipitation. Compared to Fig. 19b, the salt precipitation area in Fig. 21 is larger. In Fig. 22a, t_i is the time point for salt precipitation emerge in the injection well. Before the salt appeared, P was consistent between the two simulations. After the salt appeared, P in the simulation considering pore blockage became larger than that without blockage. In Fig. 22b, the additional pressure build-up in the blockage model from t_i, and the maximum pressure build-up (ΔP) is nearly 4.55 kPa between the two simulations.

We display the facies distribution and number the grid from 1 to 12 near the well (Fig. 23). Grids 10 to 12 are low permeability rock facies. The gas phase will invade high permeability facies (grids 1 to 9) and keep the low permeability facies brine saturation. The solid mainly produce in these high permeability zones if we do not consider the porosity or permeability changes due to the salt precipitation (Fig. 19b). Pressure is built up when we consider the porosity or permeability changes due to the salt precipitation. This makes the low permeability zone reach the initial gas entry pressure (P_0), and the dry-out process will continue to the low permeability zone (grids 10 to 12). The solid distribution will be more even around the injection well, reducing injectivity.

Salt precipitation not only affects the S_s but also the porosity of the core. If salt blocks the CO_2 flow path, salt precipitation may cause the additional pressure build-up. A more novel conclusion is that the reduction in porosity due to salt precipitation could extend the dry-out process in the low permeability zone, further expanding the salt precipitation area.

Conclusions

This article considered the recent controversies about salt migration and the influence of salt precipitation in $scCO_2$ storage in deep saline aquifers. The key role of back-flow and heterogeneity was confirmed using numerical simulation. We built homogeneous models and layered heterogeneous models to investigate the salt precipitation phenomenon, and then built a

field-scale heterogeneous model to do the simulation. The main conclusions obtained from this study are:

- The back-flow phenomenon plays an extremely important role in the formation of salt precipitation. In the short homogeneous model simulation, brine water is brought back due to capillary pressure as the supply of salt for the continuous dry-out process near the well. But this did not reach the limit of the capillary backflow at the monitoring point. In the long homogeneous model simulation, more brine is brought back to the same location. The comparison between the long homogeneous model simulation results and the results from the short cores indicate that the small size of a short core may not have enough brine source for salt precipitation. This may explain why laboratory experiments with different core scales have different results regarding salt precipitation.
- During numerical simulation, the low water content in the relative permeability function and the capillary function could have substantial effects on S_s. The low water content in the dry-out process should not be ignored during the numerical simulation, especially in the simulation of long-term injection processes. The full range of capillary function and permeability function should be chosen when it comes to simulations of dry-out problems near the well, where completely dry conditions could occur. The equation does not consider that low water content could underestimate the amount of salt precipitation.
- The heterogeneity of the matrix not only affects the distribution of salt precipitation but also the amount of salt precipitation. Results from the core-scale heterogeneous model simulation show that the extra brine at low permeability regions could serve as brine sources to supply brine for the dry-out process in high permeability regions. This leads to an increase in the amount of precipitation in the preferential flow region. The heterogeneous model is a more realistic representation of the effects of salt precipitation in the field-scale simulation. It produces more realistic phase distributions, and the maximum solid saturation value near the injection well, which is important for estimating the well injectivity.
- The generation of salt precipitation affects both the S_s and also the porosity of the core. If the salt blocks the flow path, the salt precipitation may cause additional pressure to build up. The reduction in porosity due to salt precipitation could extend the dry-out process in the low permeability zone, further expanding the salt precipitation area.

Acknowledgements

The research was supported by the Fundamental Research Funds for the Central Universities (no. 2015B26514), the Postgraduate Research and Practice Innovation Program of Jiangsu Province (no. KYCX170470), and the Fundamental Research Funds for the Central Universities (no. 2017B648X14).

References

1. Jin HG, Wood A and Seiler A, Roadmap for Carbon Capture and Storage Demonstration and Deployment in the People's Republic of China. Working paper Asian Development Bank (2015). 2. Hurter S, Labregere D, Berge J and Desitter A, Impact of mutual solubility of H2O and CO2 on injection operations for geological storage of CO2. International Conference of the Properties of Water and Steam ICPWS, Berlin (2008). 3. Baumann G, Henninges J and De Lucia M, Monitoring of saturation changes and salt precipitation during CO2 injection using pulsed neutron-gamma logging at the Ketzin pilot site. Int J Greenhouse Gas Control 28:134–146 (2014). 4. Grude S, Landrø M and Dvorkin J, Pressure effects caused by CO2 injection in the Tubåen Fm., the Snøhvitfield. Int J Greenhouse Gas Control 27:178–187 (2014). 5. Bacci G, Korre A and Durucan S, Experimental investigation into salt precipitation during CO2 injection in saline aquifers. Energy Procedia 4:4450–4456 (2011). 6. Peysson Y, Andre L and Azaroual M. Well injectivity during CO2 storage operations in deep saline aquifers – Part 1: Experimental investigation of drying effects, salt precipitation and capillary forces. Int J Greenhouse Gas Control 22:291–300 (2014). 7. Roels S M, El Chatib N, Nicolaides C and Zitha Pacelli LJ, Capillary-driven transport of dissolved salt to the drying zone during CO2 injection in homogeneous and layered porous media. Transp Porous Media 111(2):411–424 (2016). 8. Muller N, Qi R, Mackie E, Pruess K and Blunt MJ, CO2 injection impairment due to halite precipitation. Energy Procedia 1(1):3507–3514 (2009). 9. Wang Y, Luce T, Ishizawa C, Shuck M, Smith K, Ott H and Appel M, Halite precipitation and permeability assessment during supercritical CO2 core flood. International Symposium of the Society of Core Analysts, Halifax, Nova Scotia, Canada (2010). 10. Ott H, de Kloe K, Taberner C, Marcelis F, Wang Y and Makurat A, Rock/fluid interaction by injection of supercritical CO2/H2S: Investigation of dry-zone formation near the injection well. International Symposium of the Society of Core Analysts, Halifax, Nova Scotia, Canada (2010) 11. Ott H, De Kloe K, Marcelis F and Makurat A, Injection of supercritical CO2 in brine saturated sandstone: Pattern formation during salt precipitation. Energy Procedia 4:4425–4432 (2011). 12. Ott H, Roels SM and De Kloe K, Salt precipitation due to supercritical gas injection: I. Capillary-driven flow in unimodal sandstone. Int J Greenhouse Gas Control 43:247–255 (2015). 13. Hurter S, Berge JG and Labregere D, Simulations for CO2 injection projects with compositional simulator. Offshore Europe. Society of Petroleum Engineers. Aberdeen, Scotland, U.K. (2007). 14. Ott H, Andrew M, Snippe J and Blunt MJ, Microscale solute transport and precipitation in complex rock during drying. Geophys Res Lett 41(23):8369–8376 (2014). 15. Bergstad M, Or D, Withers PJ and Shokri N, The influence of NaCl concentration on salt precipitation in heterogeneous porous media. Water Resour Res 53(2):1702–1712 (2017). 16. Veran-Tissoires S and Prat M, Evaporation of a sodium chloride solution from a saturated porous medium with efflorescence formation. J Fluid Mech 749:701–749 (2014). 17. Miri R, van Noort R, Aagaard

P and Hellevang H, New insights on the physics of salt precipitation during injection of CO2 into saline aquifers. Int J Greenhouse Gas Control 43:10–21 (2015). 18. Pruess K and Müller N, Formation dry-out from CO2 injection into saline aquifers: 1. Effects of solids precipitation and their mitigation. Water Resour Res 45(3):W03402 (2009). 19. Kim KY, Han WS, Oh J, Kim T and Kim JC, Characteristics of salt-precipitation and the associated pressure build-up during CO2 storage in saline aquifers. Transp Porous Media 92(2):397–418 (2012). 20. Wasch LJ, Wollenweber J and Tambach TJ, A novel concept for long-term CO2 sealing by intentional salt clogging. Greenhouse Gases Sci Technol 3(6):491–502 (2013). 21. André L, Peysson Y and Azaroual M, Well injectivity during CO2 storage operations in deep saline aquifers – Part 2: Numerical simulations of drying, salt deposit mechanisms and role of capillary forces. Int J Greenhouse Gas Control 22:301–312 (2014). 22. Guyant E, Han WS, Kim KY, Park MH and Kim BY, Salt precipitation and CO2/brine flow distribution under different injection well completions. Int J Greenhouse Gas Control 37:299–310 (2015). 23. Wang Y, Ren J, Hu S and Di F, Global sensitivity analysis to assess salt precipitation for CO2 geological storage in deep saline aquifers. Geofluids 2017(4):1–16 (2017). 24. Pruess K, ECO2N: A TOUGH2 Fluid Property Module for Mixtures of Water, NaCl, and CO2. Lawrence Berkeley National Laboratory, Berkeley, CA (2005). 25. Basirat F, Fagerlund F, Denchik N, Pezard PA and Niemi A, Numerical modelling of CO2 injection at small-scale field experimental site in Maguelone, France. Int J Greenhouse Gas Control 54:200–210 (2016). 26. Wang Y and Liu Y, Impact of capillary pressure on permeability impairment during CO2 injection into deep saline aquifers. J Cent S Univ 20(8):2293–2298 (2013). 27. Corey AT, The interrelation between gas and oil relative permeabilities. Prod Mon 19(1):38–41 (1954). 28. Pickens JF, Gillham RW and Cameron DR, Finite-element analysis of the transport of water and solutes in title-drained soils. J Hydrol 40(3–4):243–264 (1979). 29. Narasimhan TN and Witherspoon PA, Numerical model for saturated-unsaturated flow in deformable porous media: 3. Applications. Water Resour Res 14(6):1017–1034 (1978). 30. Milly PCD, Moisture and heat transport in hysteretic, inhomogeneous porous media: A matric head-based formulation and a numerical model. Water Resour Res 18(3):489–498 (1982). 31. Van Genuchten MT, A closed-form equation for predicting the hydraulic conductivity of unsaturated soils. Soil Sci Soc Am J 44(5):892–898 (1980). 32. Das DB and Mirzaei M, Dynamic effects in capillary pressure relationships for two-phase flow in porous media: Experiments and numerical analyses. AIChE J 58(12):3891–3903 (2012). 33. Das DB and Mirzaei M, Experimental measurement of dynamic effect in capillary pressure relationship for two-phase flow in weakly layered porous media. AIChE J 59(5):1723–1734 (2013). 34. Das DB, Gill BS, Abidoye LK and Khudaida KJ, A numerical study of dynamic capillary pressure effect for supercritical carbon dioxide-water flow in porous domain. AIChE J 60(12):4266–4278 (2014). 35. Goel G, Das DB, Abidoye LK and Chahar BR, Scale dependency of dynamic relative permeability curves in relations with fluid viscosity and dynamic capillary pressure effect. Environ Fluid Mech

16(5):945–963 (2016). 36. Hanspal NS and Das DB, Dynamic effects on capillary pressure–saturation relationships for two-phase porous flow: Implications of temperature. AIChE J 58(6):1951–1965 (2012). 37. Khudaida KJ and Das DB, A numerical study of capillary pressure–saturation relationship for supercritical carbon dioxide (CO2) injection in deep saline aquifer. Chem Eng Res Des 92(12):3017–3030 (2014). 38. Abidoye LK, Khudaida KJ and Das DB, Geological carbon sequestration in the context of two-phase flow in porous media: a review. Crit Rev Environ Sci Technol 45(11):1105–1147 (2015). 39. Webb SW, A simple extension of two-phase characteristic curves to include the dry region. Water Resour Res 36(6):1425–1430 (2000). 40. Zhang ZF, Soil water retention and relative permeability for conditions from oven-dry to full saturation. Vadose Zone J 10(4):1299–1308 (2011). 41. Zhang ZF, Oostrom M, White MD, Relative permeability for multiphase flow for oven-dry to full saturation conditions. Int J Greenhouse Gas Control 49:259–266 (2016). 42. Pruess K, Oldenburg CM and Moridis GJ, TOUGH2 User's Guide Version 2. Lawrence Berkeley National Laboratory, Berkeley, CA (1999). 43. Clayton D and Andre J, GSLIB – Geostatistical Software Library and User's Guide. Oxford University Press, New York (1998). 44. Mualem Y, A new model for predicting the hydraulic conductivity of unsaturated porous media. Water Resour Res 12(3):513–522 (1976). 45. Huang DD and Honarpour MM, Capillary end effects in core flood calculations. J Pet Sci Eng 19(1–2):103–117 (1998). 46. Azaroual M, Andre L, Peysson Y, Pironon J, Broseta D, Dedecker F et al., Behaviour of the CO2 injection well and the near wellbore during carbon dioxide injection in saline aquifers. TOUGH Symposium 2012: Session V: Carbon Dioxide Storage II. Berkeley, CA (2012). 47. Zhang ZF, Soil Water Retention and Relative Permeability for Full Range of Saturation. Pacific Northwest National Laboratory (PNNL), Richland, WA (US) (2010). 48. Finsterle S, Enhancements to the TOUGH2 Simulator Integrated in iTOUGH2. Lawrence Berkeley National Laboratory, Berkeley, CA (2015). 49. Luckner L, Van Genuchten MT, Nielsen DR, A consistent set of parametric models for the two-phase flow of immiscible fluids in the subsurface. Water Resour Res 25(10):2187–2193 (1989). 50. Doughty C and Pruess K, Modeling supercritical carbon dioxide injection in heterogeneous porous media. Vadose Zone J 3(3):837–847 (2004). 51. Yang L, Numerical Simulation of CO2 Migration in Multi-scale, Heterogeneous Deep Saline Aquifers. Hohai University, Nanjing, China (2014). (In Chinese.) 52. Daher I, Salt Transport Experiments in Fractured Media. Imperial College London, London (2016). 53. Carle S F, T-PROGS: Transition Probability Geostatistical Software. University of California, Davis, CA (1999). 54. Verma A and Pruess K, Thermohydrological conditions and silica redistribution near high-level nuclear wastes emplaced in saturated geological formations. J Geophys Res: Solid Earth 93(B2):1159–1173 (1988).